

**Bubble-based stabilization for the Helmholtz equation**

Journal:	<i>International Journal for Numerical Methods in Engineering</i>
Manuscript ID:	NME-Mar-06-0209
Wiley - Manuscript type:	Research Article
Date Submitted by the Author:	22-Mar-2006
Complete List of Authors:	Harari, Isaac; Tel Aviv University, Solid Mechanics, Materials, and Systems Gosteev, Kirill; Tel Aviv University, Solid Mechanics, Materials, and Systems
Keywords:	acoustics, finite elements, stabilized methods, bubbles

powered by ScholarOne
Manuscript Central™

INTERNATIONAL JOURNAL FOR NUMERICAL METHODS IN ENGINEERING

Int. J. Numer. Meth. Engng 2000; 00:1–6Prepared using *nmeauth.cls* [Version: 2002/09/18 v2.02]

Bubble-based stabilization for the Helmholtz equation

Isaac Harari* and Kirill Gosteev

Department of Solid Mechanics, Materials and Systems, Tel Aviv University, 69978 Ramat Aviv, Israel

SUMMARY

A comparison of two bubble-enriched methods, derived by different considerations, indicates that the methods are identical in some cases. Thus, series representations of auxiliary functions, derived independently for the two methods, turn out to be equivalent prior to truncation. Three such series for time-harmonic acoustics are considered. Dispersion analysis points to the more efficient series representation and provides guidelines for the number of terms to be retained. Numerical tests confirm the validity of these practical guidelines. Copyright © 2000 John Wiley & Sons, Ltd.

KEY WORDS: acoustics; finite elements; stabilized methods; bubbles

1. INTRODUCTION

This paper considers two bubble-based methods for the stabilization of finite element computation for the Helmholtz equation, which describes time-harmonic acoustic and electromagnetic waves. The indefinite Helmholtz operator may lose ellipticity with increasing wave number, since in that case its weak form no longer induces a norm. This is related to the pollution effect, in which Galerkin finite element solutions with continuous low-order piecewise polynomials differ significantly from the best approximation [1], due to spurious dispersion in the computation, unless the mesh is sufficiently refined. In practical terms, pollution leads to a substantial increase in the cost of the finite element solution of the Helmholtz equation at higher wave numbers.

The use of element-level bubble functions to stabilize finite element computation originated over twenty years ago (see, e.g., [2]). Bubble-enhanced methods, related to stabilized finite element methods [3], are seen as arising from a separation of scales according to the numerical mesh size [4]. The residual-free bubbles (RFB) method [5, 6, 7] may be viewed as one approach to represent the fine, unresolved, scales, within the Variational Multiscale (VMS) framework [8, 9]. The link of RFB to other VMS representations of fine scales was explored in [10].

The property of best approximation indicates that a finite element solution is of minimal error in some norm. In geometric terms, the optimal finite element solution is the projection of

*Correspondence to: Isaac Harari, Department of Solid Mechanics, Materials and Systems, Tel Aviv University, 69978 Ramat Aviv, Israel

the exact solution on the finite element function space. The standard Galerkin method for the Laplace operator is optimal in the energy norm—the H^1 seminorm. This property assures good performance of the computation at any mesh refinement, i.e., high coarse-mesh accuracy. The nearly-optimal Petrov-Galerkin (NOPG) method, developed as a general methodology and applied to the Helmholtz equation [11] is motivated by the desire to achieve high coarse-mesh accuracy via best approximation in the H^1 seminorm. Such Petrov-Galerkin formulations are known [12], but generally require global weighting functions which are extremely difficult to find. The practical need for effective methods with local character leads to the NOPG method which approximates H^1 optimality. In some cases, such as in the absence of distributed sources, with piecewise linear basis functions on regular meshes, the NOPG formulation yields nodal results that are identical to those obtained by RFB. The application of these two bubble-based stabilization methods, RFB and NOPG, to the Helmholtz equation is the main focus of this paper.

The remainder of this paper is organized as follows. Section 2 presents the RFB method in the context of the VMS framework. The NOPG method, motivated by the goal of best approximation, is described in Sec. 3. Section 4 demonstrates that the application of the two methods for problems of time-harmonic acoustics is identical in many cases of interest, and presents three series representations of the bubbles for bilinear quadrilateral elements. Dispersion analysis in Sec. 5 indicates which of the bubble representations is more efficient and the number of terms to be retained in the truncated series. The dispersion performance of the bubble-enriched methods is then compared to the standard Galerkin method and least-squares stabilized methods. Section 6 reports on a series of computations examining the numerical performance of the methods, and validating the choice of series representation and the guidelines for determining the number of terms. Conclusions are offered in Sec. 7.

2. MULTISCALE APPROACH: RESIDUAL-FREE BUBBLES

Let $\Omega \subset \mathbb{R}^d$ be a d -dimensional, open, bounded region with smooth boundary Γ .

2.1. An abstract Dirichlet problem

For simplicity, we consider the following (homogeneous) Dirichlet boundary-value problem: find $u: \bar{\Omega} \rightarrow \mathbb{R}$ such that

$$\mathcal{L}u = f \quad \text{in } \Omega \quad (1)$$

$$u = 0 \quad \text{on } \Gamma \quad (2)$$

Here, $f: \Omega \rightarrow \mathbb{R}$ is given. We think of \mathcal{L} as a second-order differential operator. Generalization of the following results to problems with other types of boundary conditions and inhomogeneous boundary data, including radiation conditions representing unbounded domains, is straightforward (see Sec. 6 for numerical results with other types of boundary conditions).

The standard variational form is stated in terms of the set of functions $\mathcal{V} = H_0^1(\Omega)$: find $u \in \mathcal{V}$ such that

$$a(v, u) = (v, f), \quad \forall v \in \mathcal{V} \quad (3)$$

where (\cdot, \cdot) is the $L_2(\Omega)$ inner product. (The form of the right-hand side assumes sufficiently smooth f .) The bilinear operator is related to the differential operator via integration by parts

$$a(v, u) = (v, \mathcal{L}u) = (\mathcal{L}^*v, u) \quad (4)$$

for sufficiently smooth $u, v \in \mathcal{V}$.

The standard finite element method is based on Galerkin approximation in terms of the set of functions $\mathcal{V}^h \subset \mathcal{V}$, typically made up of continuous piecewise polynomials: find $u^h \in \mathcal{V}^h$ such that

$$a(v^h, u^h) = (v^h, f), \quad \forall v^h \in \mathcal{V}^h \quad (5)$$

This approach is optimal for the Laplace operator in the sense that it minimizes the error in the energy norm—the H^1 seminorm in this case. This property assures good performance of the computation at any mesh resolution, i.e., high coarse-mesh accuracy. However, good numerical performance at any mesh resolution is not guaranteed by the standard finite element method for other cases. In such cases, finite element computation can become prohibitively expensive in the presence of sharp gradients and rapid oscillations.

2.2. Variational multiscale framework

Numerous approaches to alleviating the above deficiency have been proposed. Inevitably, these are based on modifications of the classical piecewise polynomial Galerkin approximation. The method of residual-free bubbles (RFB) may be viewed as one of several such related methods that can be derived by the Variational Multiscale (VMS) approach [8, 9].

By this method we consider an overlapping sum decomposition of the solution. In finite element computation we have

$$\bar{u}^h = u^h + u^B \quad (6)$$

Here, $u^h \in \mathcal{V}^h$ is based on standard, finite element polynomials, representing coarse scales that are resolved by the mesh, and $u^B \in \mathcal{V}^B$ is an enhancement or enrichment, representing fine or subgrid scales, so that

$$\bar{\mathcal{V}}^h = \mathcal{V}^h \oplus \mathcal{V}^B \quad (7)$$

Such a decomposition of the solution into a linear part and a bubble was already considered in [4]. The determination of the fine scales is key to the multiscale representation. Various implementations approach this issue in different ways (see Sec. 2.3).

Following [9], we substitute the overlapping sum (6) (and its weighting function counterpart) into the variational formulation (5), to obtain a decomposed form of the variational multiscale representation

$$a(v^h, u^h) + (\mathcal{L}^*v^h, u^B) = (v^h, f) \quad (8)$$

$$a(v^B, u^h) + a(v^B, u^B) = (v^B, f) \quad (9)$$

The second term in the left-hand side of Eqn. (8) is integrated by parts, leading to a interpretation of \mathcal{L}^*v^h as a Dirac distribution on the entire domain, with integrals over element interiors and jump terms integrated across element boundaries (see [9] for details).

Equation (9) provides a formula for the unresolved, fine scales

$$u^B = M^B(\mathcal{L}u^h - f) \quad (10)$$

in terms of the integral, generally nonlocal, operator M^B which depends on the space of fine scales (again, see [9] for details). The unresolved scales may be viewed as being driven by the residual of the resolved scales.

This formula is substituted into Eqn. (8) to eliminate the fine scales from the formulation

$$a(v^h, u^h) + (\mathcal{L}^* v^h, M^B \mathcal{L} u^h) = (v^h, f) + (\mathcal{L}^* v^h, M^B f) \quad (11)$$

This is an equation for the coarse scales, which includes the nonlocal effect of the fine scales.

2.3. The fine scales

Various practical approximations arise from different treatments of the unresolved, fine scales.

The simplest approach is to employ a bubble representation of the fine scales [3, 4, 13], thereby omitting the inter-element jump terms and localizing the effect of the fine scales. Solving a homogeneous Dirichlet, element-level, problem for the fine scales is the approach that underlies the concept of residual-free bubbles [5, 6, 7], as well as the related method of nearly optimal Petrov-Galerkin (NOPG) [11, 14]. The application of these two bubble-based stabilization methods, RFB and NOPG, is the main focus of this paper. A similar result is obtained by employing an element Green's function [8], and the link to RFB was explored in [10]. The obvious limitation related to the loss of essential global effects inherent in local approaches may be overcome by employing nonconforming methods [15, 16]. The relationship of VMS methods based on *fine-scale* Green's functions to optimal stabilized methods with global and local character is described in [17].

Stabilized methods of adjoint type, also called 'unusual stabilized finite element methods' [18, 19], may be derived in the VMS framework as well, and are related to RFB. The structure of the second term on the left-hand side of Eqn. (11) indicates that the stability parameter provides an algebraic approximation of the integral operator M^B . The VMS distributional interpretation motivated the development of a stabilized method that includes the inter-element jump terms [20], that are usually omitted in the local approach.

An alternative approach that has appeared predominantly in time-harmonic acoustic applications is to base the fine scales on free-space solutions of the homogeneous differential equation (for example, plane waves in the case of the Helmholtz equation). These functions are often readily available, but typically global and hence require specialized treatment in practice. The discontinuous enrichment method (DEM) [21, 22] retains standard finite element polynomials for the coarse scales, enriched within each element by nonconforming free-space homogeneous solutions representing fine scales, with Lagrange multipliers enforcing inter-element continuity in the variational formulation.

2.4. Residual-free bubbles

Partition Ω in the usual way into n_{el} non-overlapping regions Ω^e (element domains) with boundaries Γ^e , $e = 1, \dots, n_{el}$. We denote the union of element interiors by

$$\tilde{\Omega} = \bigcup_{e=1}^{n_{el}} \Omega^e \quad (12)$$

Similarly, the union of element boundaries is denoted

$$\tilde{\Gamma} = \bigcup_{e=1}^{n_{el}} \Gamma^e \quad (13)$$

We assume that \mathcal{V}^h is given, and that the enrichment functions u^B (and v^B) are element-level bubbles, i.e., vanish at element interfaces. Equation (9) can then be written in strong form

$$\mathcal{L}u^B = -(\mathcal{L}u^h - f) \quad \text{in } \tilde{\Omega} \quad (14)$$

$$u^B = 0 \quad \text{on } \tilde{\Gamma} \quad (15)$$

In this case, Eqn. (8) is simplified since the inter-element jumps in the second term on the left-hand side vanish due to the bubble nature of the enrichment functions leaving only integrals over element interiors

$$a(v^h, u^h) + (\mathcal{L}^*v^h, u^B)_{\tilde{\Omega}} = (v^h, f) \quad (16)$$

The subscript on the inner product denotes a domain of integration other than Ω . This is the RFB problem, with the residual-free bubbles defined in (14) and (15).

Remark This form of the equation justifies the use of simplifications of u^B in practical implementation. For advection-diffusion, a reduced solution for the advective limit is considered, lacking a thin boundary layer along the outflow boundary to satisfy compatibility requirements. The presence of such a boundary layer is of little consequence in the integration of the bubble in Eqn. (16), so that it may be neglected in practice.

The basis for \mathcal{V}^B is defined on the element level, in terms of N_a , the standard polynomial shape function of local node a . Since u^h in an element is expressed as a linear combination of nodal polynomial shape functions and nodal coefficients, u^B is also expressed as a linear combination of nodal bubble basis functions b_a and the same nodal coefficients. The bubble basis functions are found by solving

$$\mathcal{L}b_a = -(\mathcal{L}N_a - f) \quad \text{in } \Omega^e \quad (17)$$

$$b_a = 0 \quad \text{on } \Gamma^e \quad (18)$$

3. BEST APPROXIMATION: NEARLY-OPTIMAL PETROV-GALERKIN METHOD

As noted in Sec. 2.1, the standard finite element approximation that results from the Galerkin method (5), is not necessarily optimal in any sense.

3.1. H^1 optimality

Following [11], we consider another improved approach. Ideally, we seek an approximate solution which is optimal in terms of the H^1 seminorm. That is, we wish to find $u^h \in \mathcal{V}^h$ such that

$$(\nabla v^h, \nabla e) = 0, \quad \forall v^h \in \mathcal{V}^h \quad (19)$$

Here $e = u^h - u$ and u is solution of (1)–(2) or (3). Generally, (19) cannot be solved for u^h , since u is unknown. A Petrov-Galerkin formulation with optimal solutions that satisfy Eqn. (19) generally requires global weighting functions which are extremely difficult to find [12].

For the special case of the Laplace operator, $\mathcal{L} = -\Delta$, the Galerkin approximation (5) leads to the H^1 projection (19), which guarantees good performance of the computation on any mesh refinement. Our goal, then, is to formulate a problem that retains optimality in the sense of (19), at least approximately, yet may be solved directly.

3.2. The nearly-optimal Petrov-Galerkin method

We assume that v^h is given. Then, for each Galerkin weighting function $v^h \in \mathcal{V}^h$, we construct a function $\bar{v}^h \in \bar{\mathcal{V}}^h \subset \mathcal{V}$ that satisfies

$$\mathcal{L}^* \bar{v}^h = \Delta v^h \quad \text{in } \tilde{\Omega} \quad (20)$$

$$\bar{v}^h = v^h \quad \text{on } \tilde{\Gamma} \quad (21)$$

We note that while the functions $v^B = \bar{v}^h - v^h$ are bubbles over the elements, they are not residual free, except in special cases such as piecewise linear Galerkin weighting functions on regular meshes.

Starting from the H^1 projection (19), we now derive our NOPG formulation :

$$\begin{aligned} (\nabla v^h, \nabla e) &= -(\Delta v^h, e)_{\tilde{\Omega}} + (\llbracket v^h \rrbracket, e)_{\tilde{\Gamma}} \\ &= -(\mathcal{L}^* \bar{v}^h, e)_{\tilde{\Omega}} + (\llbracket v^h \rrbracket, e)_{\tilde{\Gamma}} \\ &= a(\bar{v}^h, e) + (\llbracket v^h - \bar{v}^h \rrbracket, e)_{\tilde{\Gamma}} \\ &= a(\bar{v}^h, u^h) - (\bar{v}^h, f) + (\llbracket v^h - \bar{v}^h \rrbracket, e)_{\tilde{\Gamma}} \end{aligned} \quad (22)$$

We used integration by parts, the definition of the modified weighting functions (20) and the fact that $\bar{\mathcal{V}}^h \subset \mathcal{V}$. Here, $\llbracket \cdot \rrbracket$ is the jump at an element boundary. Equation (22) motivates the following NOPG problem: Find $u^h \in \mathcal{V}$ such that

$$a(\bar{v}^h, u^h) = (\bar{v}^h, f), \quad \forall \bar{v}^h \in \bar{\mathcal{V}}^h \quad (23)$$

The modified weighting functions are defined in (20) and (21).

The label ‘nearly-optimal’ can be justified by the fact that this formulation approximates the H^1 -optimal result (19), in the sense that its solution satisfies

$$(\nabla v^h, \nabla e) = (\llbracket v^h - \bar{v}^h \rrbracket, e)_{\tilde{\Gamma}} \quad (24)$$

The non-zero right-hand side is a measure of the distance of the Petrov-Galerkin solution from H^1 -optimality. This is related to the lack of symmetry of the formulation.

The basis for $\bar{\mathcal{V}}^h$ is defined on the element level, in terms of the standard local shape functions N_a . Since v^h in an element is expressed as a linear combination of nodal shape functions and arbitrary nodal coefficients, \bar{v}^h is also expressed as a linear combination of modified nodal shape functions \bar{N}_a and the same arbitrary nodal coefficients. The modified shape functions are found by solving

$$\mathcal{L}^* \bar{N}_a = -\Delta N_a \quad \text{in } \Omega^e \quad (25)$$

$$\bar{N}_a = N_a \quad \text{on } \Gamma^e \quad (26)$$

The modified shape functions retain the interpolation property of the standard polynomial shape functions.

4. BUBBLE ENRICHMENT: TIME-HARMONIC ACOUSTICS

The RFB and NOPG improved methods, obtained by bubble-based enrichment, are closely related, and identical in some cases.

4.1. Comparison of the methods

The approximate solution in the RFB method (16) is enriched by the residual-free bubble u^B , whereas the weighting function in the NOPG method (23) is replaced by a modified weighting function \bar{v}^h . In order to compare the two methods, recall that the RFB method can be written in terms of a modified approximate solution

$$\bar{u}^h = u^h + u^B \quad (27)$$

and the the modified weighting function of NOPG can be expressed in terms of a bubble

$$\bar{v}^h = v^h + v^B \quad (28)$$

In both cases, the nodal basis can be formed either in terms of modified shape functions, or bubble basis functions

$$\bar{N}_a = N_a + b_a \quad (29)$$

Thus, the modified shape function can be defined directly, or via the bubble basis function.

The element-level auxiliary boundary-value problem that define the RFB modified shape functions is

$$\mathcal{L}\bar{N}_a = f \quad \text{in } \Omega^e \quad (30)$$

$$\bar{N}_a = N_a \quad \text{on } \Gamma^e \quad (31)$$

and for NOPG

$$\mathcal{L}^*\bar{N}_a = -\Delta N_a \quad \text{in } \Omega^e \quad (32)$$

$$\bar{N}_a = N_a \quad \text{on } \Gamma^e \quad (33)$$

Alternatively, the RFB bubble basis functions satisfy

$$\mathcal{L}b_a = -(\mathcal{L}N_a - f) \quad \text{in } \Omega^e \quad (34)$$

$$b_a = 0 \quad \text{on } \Gamma^e \quad (35)$$

whereas for NOPG

$$\mathcal{L}^*b_a = -(\mathcal{L}^* + \Delta)N_a \quad \text{in } \Omega^e \quad (36)$$

$$b_a = 0 \quad \text{on } \Gamma^e \quad (37)$$

The boundary conditions for both methods, either in terms of modified shape functions or bubble basis functions, are identical, and the governing differential equations are quite similar.

The difference in the differential operator is removed for self-adjoint operators such as the Helmholtz operator, $\mathcal{L}u = -\Delta u - k^2u$ with given wave number k , governing time-harmonic acoustics that are considered in the following.

The remaining differences between the auxiliary functions of the two methods lie in the presence of the given function f and the Laplacian of the standard shape function ΔN_a . The auxiliary functions may be derived analytically [6, 11] or numerically [7, 23]. Analytical solutions of the element-level boundary-value problem are obtained on elements of simple shapes (squares or rectangles) for the homogeneous equation, i.e., the functions for the two methods are identical. Auxiliary functions that are obtained analytically may be used

in computations in elements of general shape as well (see Sec. 6 for numerical results on unstructured meshes).

Many problems of acoustics are governed by the homogeneous Helmholtz equation, in which $f = 0$. The performance of numerical methods for problems of acoustics is often evaluated by dispersion analysis, which examines homogeneous solutions on regular meshes. Under these conditions, again, the functions for the two methods are identical.

Remark In many cases the two methods with identical auxiliary functions lead to the same nodal solutions. However, the RFB solution is enriched with bubbles, whereas the NOPG solution is not. Thus, the RFB method may exhibit superior performance measured in an integral norm (see Sec. 6).

In summary, the auxiliary functions are expressed either by modified shape functions that satisfy a homogeneous Helmholtz equation within the element with inhomogeneous Dirichlet boundary conditions on the element boundary

$$\mathcal{L}\bar{N}_a = 0 \quad \text{in } \Omega^e \quad (38)$$

$$\bar{N}_a = N_a \quad \text{on } \Gamma^e \quad (39)$$

or by bubble basis functions that satisfy an inhomogeneous Helmholtz equation within the element with homogeneous Dirichlet boundary conditions on the element boundary

$$\mathcal{L}b_a = k^2 N_a \quad \text{in } \Omega^e \quad (40)$$

$$b_a = 0 \quad \text{on } \Gamma^e \quad (41)$$

We now present expressions for the auxiliary functions in one and two dimensions. These were previously derived independently, without recognizing the connection between them.

4.2. Linear interpolation in one dimension

We begin with two-noded linear element of length h in one dimension, $a = 1$ or 2 . The parent domain is the biunit interval with nodal coordinate $\xi_a = (-1)^a$. The linear shape functions are

$$N_a = \frac{1}{2}(1 + \xi_a \xi), \quad a = 1, 2 \quad (42)$$

The modified shape functions [11]

$$\bar{N}_a = \frac{\sin(khN_a(\xi))}{\sin kh} \quad (43)$$

are expressed concisely in terms of the linear shape functions, satisfying the element-level boundary-value problem (38) and (39). As expected, $\bar{N}_a \rightarrow N_a$ as $kh \rightarrow 0$.

The modified shape functions become unbounded at $kh = \pi$, the first resonance of the boundary-value problem (38) and (39). This corresponds to an unrealistically low mesh resolution of $G = 2$ ($G = 2\pi/(kh)$ represents the number of nodal points per wave length), and thus poses no practical difficulty.

As a prelude to the more complicated two dimensional configurations, consider an alternative representation for the one-dimensional case as an infinite series for the bubbles. The bubble basis function is expressed in terms of eigenfunctions of the Dirichlet problem for the Laplacian

$$b_a = \sum_{n=1}^{\infty} A_n \sin(n\pi N_a(\xi)) \quad (44)$$

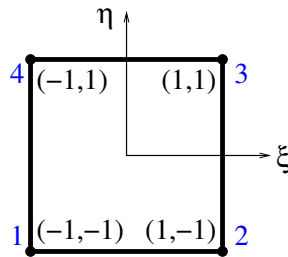


Figure 1. Parent domain of a bilinear element.

satisfying the homogeneous boundary conditions (41). In order to satisfy the inhomogeneous differential equation (40), by orthogonality

$$A_n = \frac{2}{n\pi} \frac{(-1)^n}{1 - \left(\frac{n\pi}{kh}\right)^2} \quad (45)$$

At resolutions over $G = 2$ (i.e., $kh < \pi$) the boundary-value problems (38)–(39) and (40)–(41) have unique solutions, so that the modified shape functions (43) and the untruncated series representation of the bubble basis functions (44) satisfy the relationship (29).

4.3. Bilinear interpolation in two dimensions

We proceed to a four-noded bilinear square element of side h in two dimensions, $a = 1, \dots, 4$. The parent domain is the biunit square with nodal coordinates (ξ_a, η_a) , see Fig. 1. The bilinear shape functions are

$$N_a = \frac{1}{2}(1 + \xi_a \xi)(1 + \eta_a \eta), \quad a = 1, \dots, 4 \quad (46)$$

Three series representation are presented for this case, starting with a simplification of a double-index series derived in a manner similar to that just presented in one dimension [11], denoted here BH. The bubble basis function is again expressed in terms of eigenfunctions of the Dirichlet problem for the Laplacian

$$b_a = \sum_{m,n=1}^{\infty} A_{mn} \sin\left(\frac{m\pi}{2}(1 + \xi_a \xi)\right) \sin\left(\frac{n\pi}{2}(1 + \eta_a \eta)\right) \quad (47)$$

satisfying the homogeneous boundary conditions (41). In order to satisfy the inhomogeneous differential equation (40), by orthogonality

$$A_{mn} = \frac{-4}{mn\pi^2} \frac{(-1)^{m+n}}{1 - (m^2 + n^2) \left(\frac{\pi}{kh}\right)^2} \quad (48)$$

In practice the series is truncated after a finite number of terms. Let M and N denote the upper limit of each index. We consider only cases in which $M = N$.

An alternative approach was employed in the first application of the RFB method to the Helmholtz equation [6], denoted here FFML. Separation of variables leads to a single-index

series for the modified shape function, satisfying the homogeneous equation (38)

$$\bar{N}_a = \sum_m^{\infty} \frac{C_m}{\sinh B_m} \left(\sin \left(\frac{m\pi}{2} (1 + \xi_a \xi) \right) \sinh \left(\frac{B_m}{2} (1 + \eta_a \eta) \right) + \sinh \left(\frac{B_m}{2} (1 + \xi_a \xi) \right) \sin \left(\frac{m\pi}{2} (1 + \eta_a \eta) \right) \right) \quad (49)$$

Here, $B_m = \sqrt{(m\pi)^2 - (kh)^2}$. In order to satisfy the inhomogeneous boundary conditions (39), by orthogonality

$$C_m = 2 \frac{(-1)^{m+1}}{m\pi} \quad (50)$$

In practice the series is truncated after M terms. Numerical tests were performed with $M = 200$ terms in this series [6, 24].

An unpublished approach [25], denoted here CF, again considers the bubble. A single-index series is obtained by separation of variables, treating the homogeneous and particular solutions in one of the directions separately and satisfying the homogeneous boundary conditions (41)

$$b_a = (kh)^2 \sum_m \frac{C_m}{B_m^2} \sin \left(\frac{m\pi}{2} (1 + \xi_a \xi) \right) \left(\frac{1}{2} (1 + \eta_a \eta) - \frac{\sinh \left(\frac{B_m}{2} (1 + \eta_a \eta) \right)}{\sinh B_m} \right) \quad (51)$$

The definitions of the coefficients B_m and C_m provided in the FFML series assure satisfaction of the inhomogeneous equation (40). Again, in practice the series is truncated after M terms.

As in the one-dimensional case, the boundary-value problems (38)–(39) and (40)–(41) have unique solutions at resolutions over $G = 2$ (i.e., $kh < \pi$). Thus the full series representations of the bubble basis functions (47) and (51) are equal, and together with the modified shape functions (49) satisfy the relationship (29).

As a practical guideline, we wish to determine which of these three alternative series, BH, FFML, or CF, provides adequate representation of the improved shape functions with the fewest terms, and the number of terms that should be used.

5. DISPERSION ANALYSIS

Dispersion analysis of numerical methods for the Helmholtz equation examines the dependence of the numerical error on mesh resolution as well as mesh orientation, by comparison to exact, free-space solutions of the constant-coefficient, homogeneous equation, typically in the form of plane waves. In the case of the RFB and NOPG methods, dispersion depends also on the number of terms employed in the series representations of the improved shape functions.

5.1. Series selection and truncation

Consider a uniform, two-dimensional mesh of four-noded elements of size h , aligned with the global axes, with nodes at (ph, qh) , $p, q \in \mathbb{Z}$. Values of a plane wave, oriented at an angle θ to the mesh, at the nodal points are

$$u(ph, qh) = (\exp(ikhc))^p (\exp(ikhs))^q \quad (52)$$

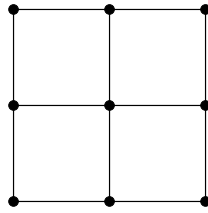


Figure 2. Nine-node patch.

Here, $i = \sqrt{-1}$ is the imaginary unit, $c = \cos \theta$ and $s = \sin \theta$. Similarly, we assume that corresponding nodal values of finite-element solutions are

$$u^h(ph, qh) = (\exp(ik^h hc))^p (\exp(ik^h hs))^q \quad (53)$$

The dependence of the approximate wave number k^h on the mesh resolution G and the orientation of the mesh with respect to the direction of propagation θ is determined by the analysis of a standard nine-node patch (Fig. 2).

As noted, in the practical implementation of the bubble-enriched methods, dispersion depends also on the number of terms employed in the series M . Let k_M^h denote the approximate wave number obtained by the truncated representation of a given series, and k^h denotes the approximate wave number obtained by the full representation of any of the series (computed by taking a large number of terms in one of the series).

The coefficients of the dispersion equation depend on the entries of the element coefficient matrix. Thus explicit expressions for the coefficient matrix that arises from each of the series representations must be formulated. Each entry is in the form of a series. Explicit expressions for these terms are available [26].

The dispersion equation can then be solved for the approximate wave number of each series representation. The relative error in the approximate wave number is

$$e = \frac{k_M^h - k^h}{k^h} \quad (54)$$

This measure is used to evaluate the convergence of each series. The relative error for each series depends also on the resolution and orientation. The dispersion error generally decreases with the increase in resolution. Dispersion in the standard Galerkin method is an even function of the orientation, with a periodicity of $\pi/2$ [27], and in the BH and FFML methods the situation is the same. Thus, the two extremes occur at $\theta = 0$ and $\theta = \pi/4$. The CF method is not symmetric in ξ and η , so that in this case the two extremes occur at $\theta = 0$ and $\theta = \pi/2$ (see [26] for details). The dependence of the relative error on the number of terms in each series, for a low resolution of $G = 4$ and an intermediate resolution of $G = 10$, and the two extreme values of orientation, is shown in Fig. 3.

The accuracy of all three series is better at the higher resolution and the difference between the two extreme orientations is smaller, to the extent that the errors of the two orientations are indistinguishable at the higher resolution of the BH series. However, in all cases, the differences between resolutions and orientations for a given series are relatively small, while there is considerable dependence on the number of terms in the series. The scale of the FFML plot is larger than the other two. While the plots of the BH and CF series seem somewhat

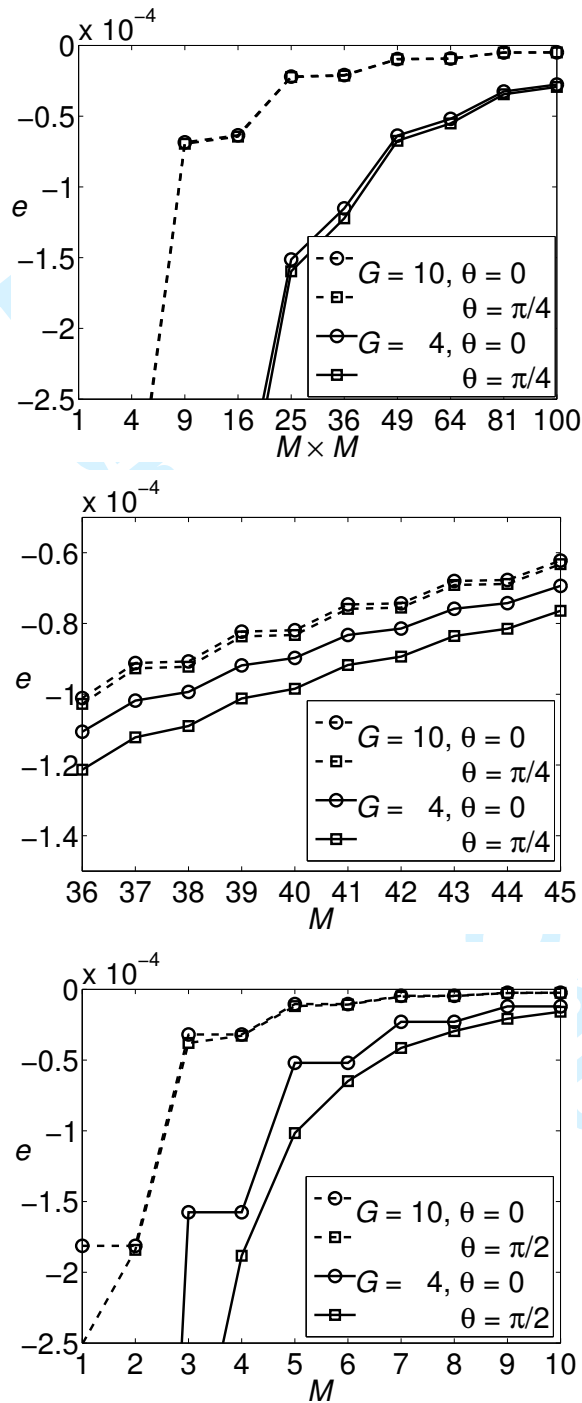


Figure 3. Relative error in the approximate wave number $e = k_M^h/k^h - 1$ of the truncated BH (top), FFML (center), and CF series.

Table I. The number of terms required in each series to bound the relative error in the approximate wave number by $e < 10^{-4}$, see Fig. 3.

G	BH	FFML	CF
10	3×3	37	3
4	7×7	40	6

similar, the number of terms in the double-indexed BH series is much larger. The CF series clearly requires the fewest terms to attain a given accuracy. The number of terms in each series required to keep the relative error in the approximate wave number below a threshold of 10^{-4} is shown in Table I. The CF series with six terms provides this accuracy at any resolution above four points per wave length. Consequently, we advocate the use of the CF series with about six terms for the four-noded RFB and NOPG elements.

5.2. Anisotropy

Now that the bubble representation has been determined, the dispersion properties of the four-noded RFB and NOPG elements can be examined. Of course, all three series representations converge to the same dispersion behavior with a sufficient number of terms.

Figure 4 shows the dependence of the relative error in wave number on the orientation of the mesh with respect to the direction of propagation, varying between the two extreme cases of propagation along element sides and along element diagonals. The reduction in dispersion of the bubble-enriched methods over the standard Galerkin method is clear, most noticeably at the lower resolutions. The particularly good performance of the improved methods along element diagonals is striking, and agrees with behavior observed in numerical tests for advection-diffusion [5].

The superior performance of the bubble-enriched methods over the Galerkin method motivates the comparison to other improved methods such as the Galerkin/least-squares (GLS) stabilized method [28]. This method contains a stability parameter which can be designed by dispersion analysis to eliminate spurious dispersion of plane waves in a specified direction of propagation [27]. Figure 5 compares the behavior of the bubble-enriched methods to that of the version of GLS that eliminates spurious dispersion along element diagonals. In this case the dispersion properties of GLS are superior at every resolution. The version of GLS that is advocated in [27] eliminates spurious dispersion of plane waves in the bisecting direction, and the comparison for this case is shown in Fig. 6. The dispersion behavior in this case is comparable. It is interesting to examine the performance predicted by the dispersion analysis in computation.

6. NUMERICAL RESULTS

A series of computations examines the numerical performance of the bubble-enriched methods, employing structured and unstructured meshes of four-noded quadrilaterals, for several wave guide problems. The bubble enrichment is based on the CF representation with six terms, as

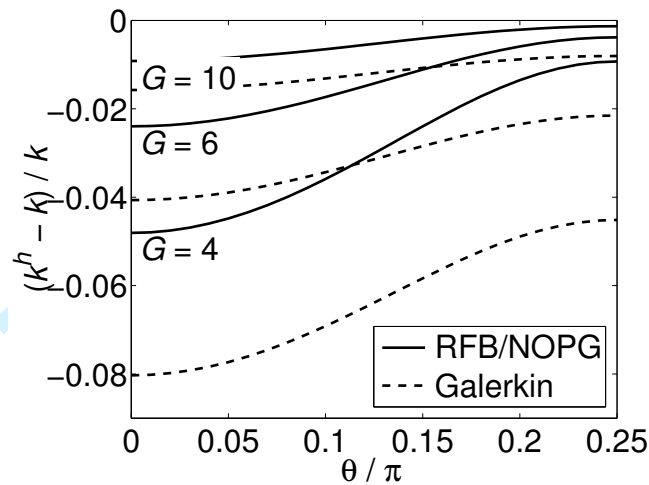


Figure 4. Dispersion error of four-noded elements: bubble-enriched and Galerkin.

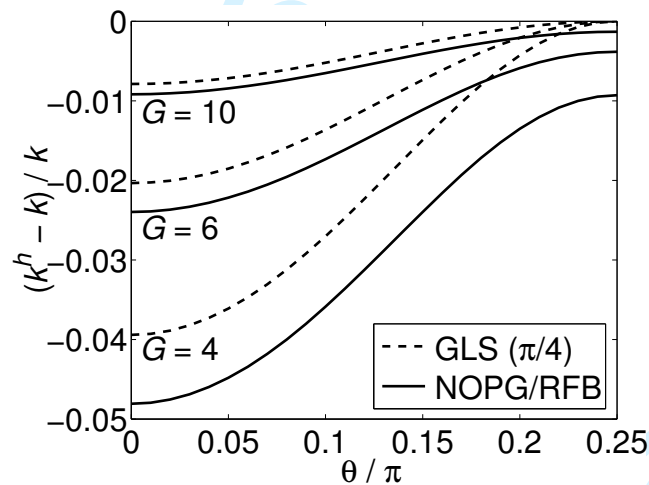


Figure 5. Dispersion error of four-noded elements: bubble-enriched and GLS (dispersion-free along diagonals).

recommended by the dispersion analysis. The behavior is compared to the version of the least-squares stabilized method that eliminates spurious dispersion of plane waves in the bisecting direction, as advocated in [27], and denoted GLS ($\pi/8$). Results of some of these numerical tests are reported.

Consider an $a \times a$ square with $ka = 8$ and no distributed sources ($f = 0$). Two cases are considered, defined by different combinations of boundary conditions (to be specified subsequently) that are imposed on the boundaries of the square so that the exact solution

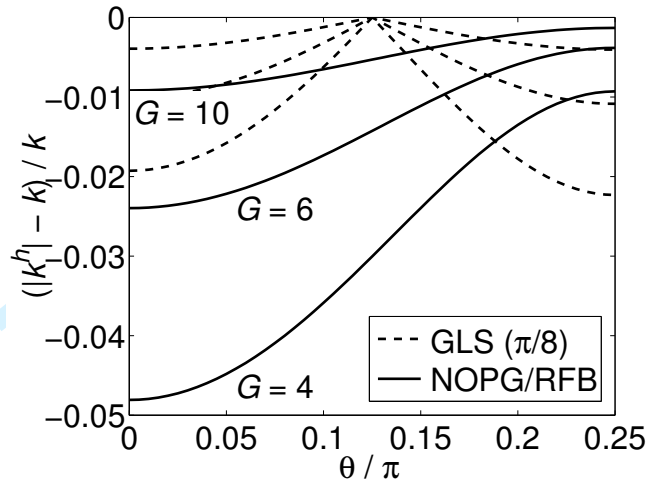


Figure 6. Dispersion error of four-noded elements: bubble-enriched and GLS (dispersion-free in bisecting direction).

is a plane wave propagating in a given direction

$$u = \exp(ik(x \cos \theta + y \sin \theta)) \quad (55)$$

The domain is discretized by three sets of three increasingly refined meshes each. The first set consists of nested uniform meshes of 8×8 , 16×16 , and 32×32 elements, i.e., the element sides are halved from one level of refinement to the next (Fig. 7). The corresponding resolutions are 6.3, 12.6, and 25.1 points per wavelength.

The other two sets consist of three non-uniform meshes each, one in a symmetric configuration (Fig. 8), and the other completely unstructured (Fig. 9). Each mesh has a mean element size roughly the same as the corresponding uniform mesh. The element size of a distorted element is taken as the average side of the element.

In the coarsest symmetric mesh there are 53 nodes with 40 quadrilaterals. The resolution in this mesh ranges from 3.6 to 11.2 (with a mean of 6.0) points per wavelength. In the intermediate symmetric mesh there are 185 nodes with 160 quadrilaterals. The resolution mesh ranges from 7.0 to 22.4 (with a mean of 12.1) points per wavelength. In the finest symmetric mesh there are 689 nodes with 640 quadrilaterals. The resolution ranges from 14.0 to 44.9 (with a mean of 24.1) points per wavelength.

In the coarsest unstructured mesh there are 97 nodes with 76 quadrilaterals. The resolution in this mesh ranges from 3.5 to 19.3 (with a mean of 8.5) points per wavelength. In the intermediate unstructured mesh there are 345 nodes with 304 quadrilaterals. The resolution ranges from 6.9 to 41.3 (with a mean of 17.1) points per wavelength. In the finest unstructured mesh there are 1297 nodes with 1216 quadrilaterals. The resolution ranges from 13.4 to 85.2 (with a mean of 34.3) points per wavelength. These meshes contain highly distorted elements with large variations in mesh size, in order to test computational performance under extreme conditions.

The bubble enrichment is originally constructed for square elements. The same functions, defined in the parent domain, are used for general quadrilateral elements as well, although they

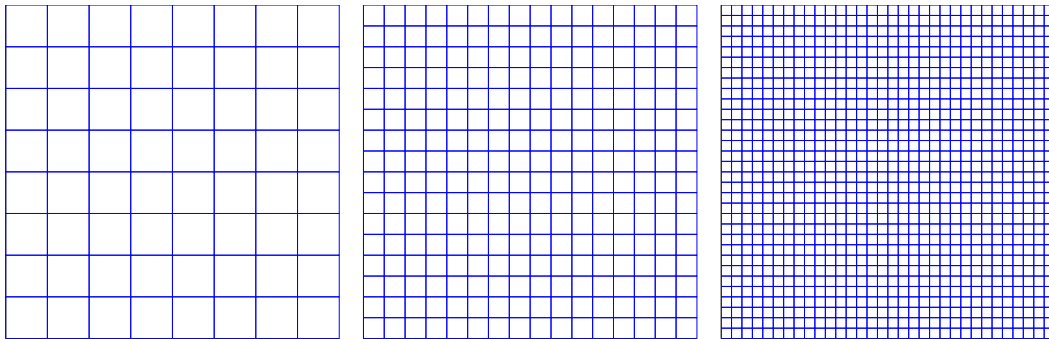


Figure 7. Uniform meshes.

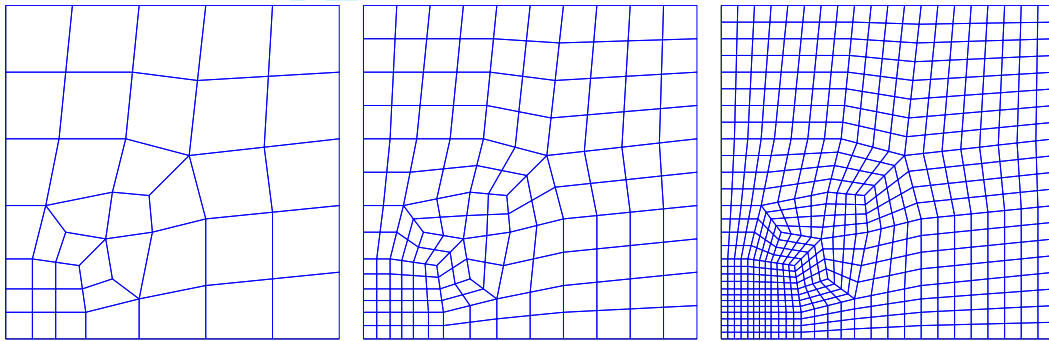


Figure 8. Symmetric meshes.

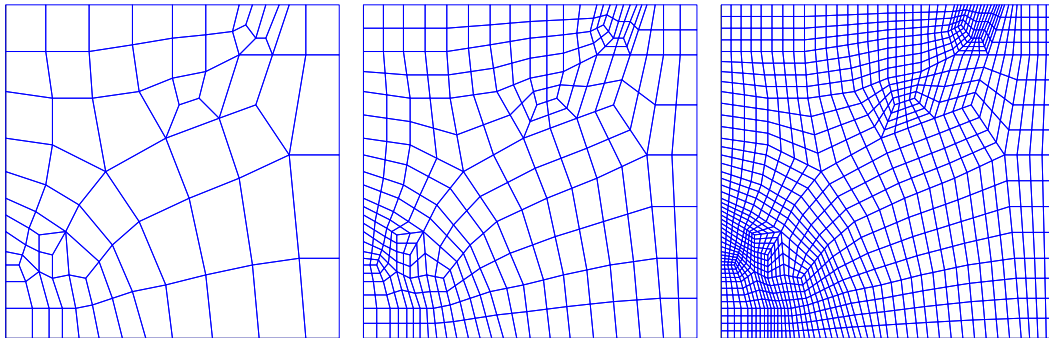


Figure 9. Unstructured meshes.

don't satisfy the auxiliary boundary-value problems exactly in distorted elements. Integration in distorted elements is performed with 2×2 Gaussian quadrature.

The first case presented is a plane wave aligned with the x -axis, i.e., $\theta = 0$ in Eqn. (55),

specified by appropriate inhomogeneous Dirichlet boundary conditions on the boundaries that are normal to the x -axis, and homogeneous Neumann boundary conditions on the boundaries that are normal to the y -axis. Results for the various meshes are reported in Fig. 10, measured in the H^1 seminorm. Nodal results of the NOPG and RFB methods on meshes that are not uniform are indistinguishable, although not theoretically identical. Accounting for the bubble enrichment in the RFB results, denoted RFB(+), considerably reduces the error norm. The RFB/NOPG results are comparable to GLS ($\pi/8$) and slightly better than the Galerkin solution, particularly at lower resolutions. However, the RFB(+) results are noticeably superior.

Inhomogeneous Robin boundary conditions are now specified on all boundaries, so that the exact solution is a plane wave propagation at an angle of $\theta = \pi/4$ with respect to the x -axis, see Eqn. (55). Results for the various meshes are reported in Fig. 11. The performance observed in the previous case is repeated here, namely that the RFB/NOPG results are comparable to GLS ($\pi/8$) and slightly better than the Galerkin solution, particularly at lower resolutions, and the RFB(+) results are noticeably superior.

7. CONCLUSIONS

The residual-free bubble (RFB) and nearly-optimal Petrov-Galerkin (NOPG) bubble-based methods stabilize finite element computation for the Helmholtz equation. Both methods are derived in the general context of an abstract problem—RFB from multiscale considerations and NOPG with the goal of providing best approximation. In their application to the Helmholtz equation, the two methods yield identical discrete formulations in many cases of interest, and their auxiliary functions satisfy the same element-level boundary-value problem. Thus series representations of the auxiliary functions derived for the two methods independently turn out to be equivalent prior to truncation. Three such series for bilinear quadrilateral elements are considered. Dispersion analysis points to the more efficient series representation and provides guidelines for the number of terms to be retained. The dispersion performance of the bubble-enriched methods is then compared to the standard Galerkin method and least-squares stabilized methods. Numerical tests examine the performance of the methods, and validate the choice of truncated series representation.

REFERENCES

1. I. Babuška, F. Ihlenburg, E. T. Paik, and S. A. Sauter. A generalized finite element method for solving the Helmholtz equation in two dimensions with minimal pollution. *Comput. Methods Appl. Mech. Engrg.*, 128(3-4):325–359, 1995.
2. D. N. Arnold, F. Brezzi, and M. Fortin. A stable finite element for the Stokes equations. *Calcolo*, 21(4):337–344, 1984.
3. F. Brezzi, M. O. Bristeau, L. P. Franca, M. Mallet, and G. Rogé. A relationship between stabilized finite element methods and the Galerkin method with bubble functions. *Comput. Methods Appl. Mech. Engrg.*, 96(1):117–129, 1992.
4. L. P. Franca and C. Farhat. Bubble functions prompt unusual stabilized finite element methods. *Comput. Methods Appl. Mech. Engrg.*, 123(1-4):299–308, 1995.
5. F. Brezzi, L. P. Franca, and A. Russo. Further considerations on residual-free bubbles for advective-diffusive equations. *Comput. Methods Appl. Mech. Engrg.*, 166(1-2):25–33, 1998.
6. L. P. Franca, C. Farhat, A. P. Macedo, and M. Lesoinne. Residual-free bubbles for the Helmholtz equation. *Internat. J. Numer. Methods Engrg.*, 40(21):4003–4009, 1997.

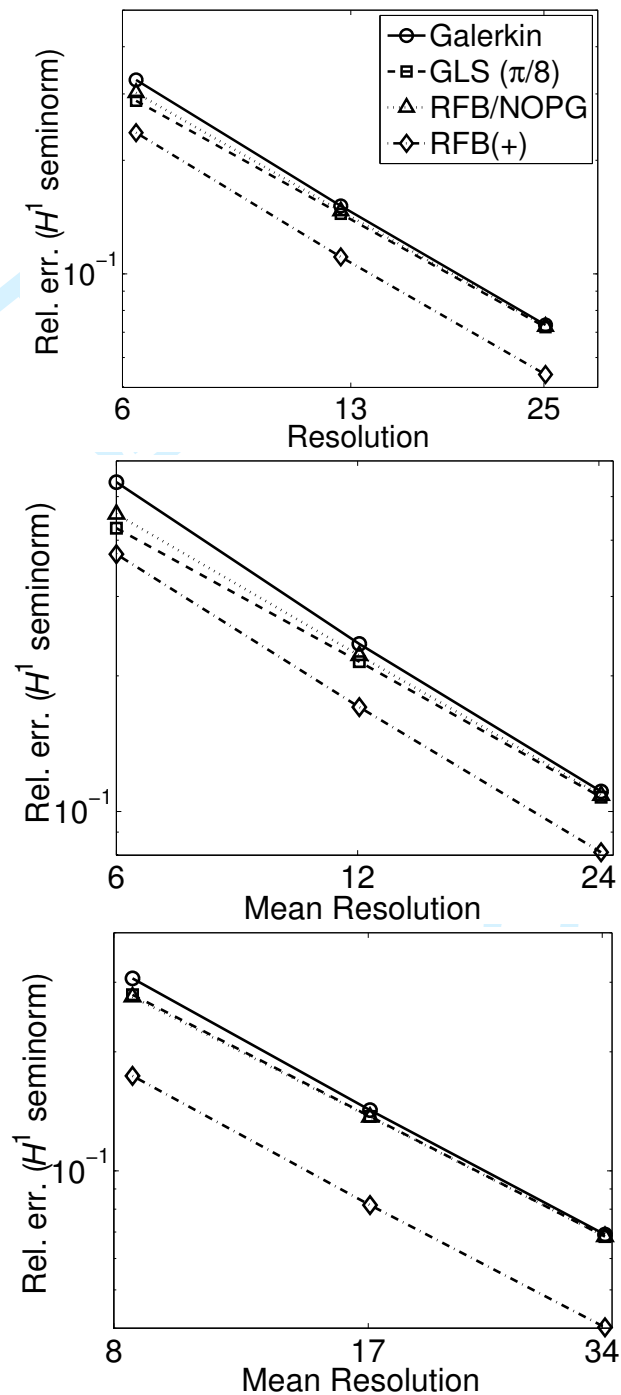


Figure 10. Wave guide at $\theta = 0$, Dirichlet-Neumann boundary conditions: structured (top), symmetric (center), and unstructured meshes.

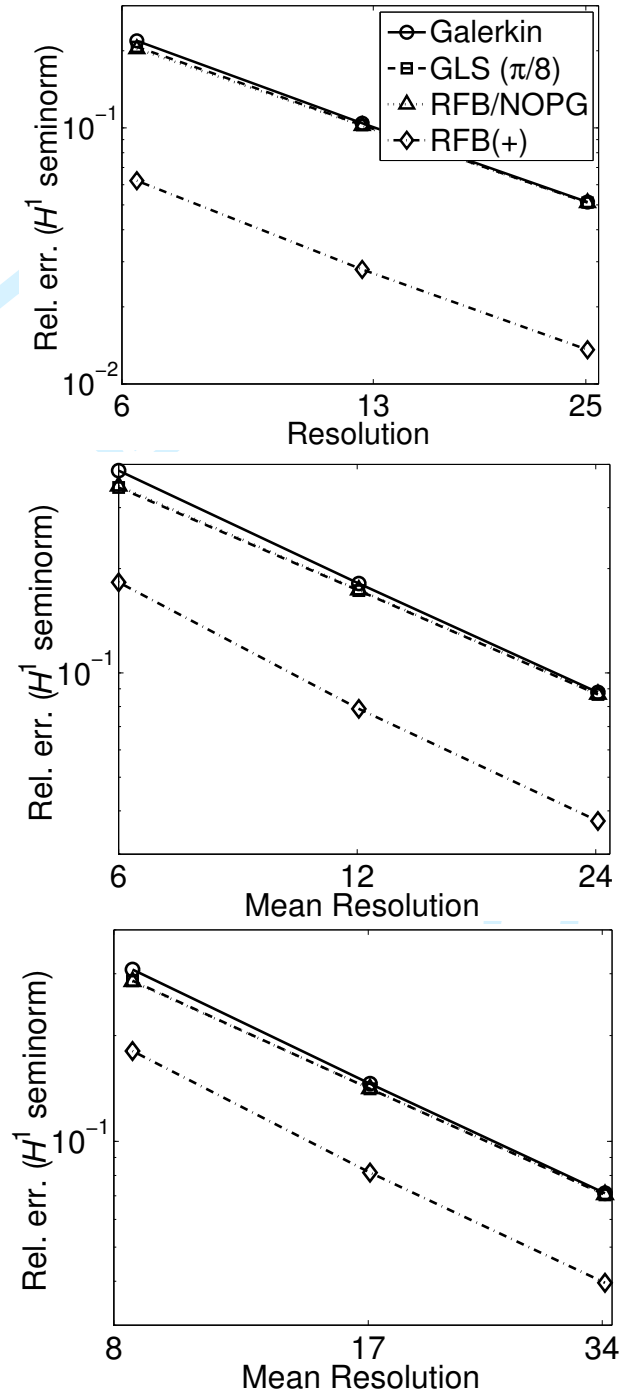


Figure 11. Wave guide at $\theta = \pi/4$, Robin boundary conditions: structured (top), symmetric (center), and unstructured meshes.

7. L. P. Franca, A. Nesliturk, and M. Stynes. On the stability of residual-free bubbles for convection-diffusion problems and their approximation by a two-level finite element method. *Comput. Methods Appl. Mech. Engrg.*, 166(1-2):35–49, 1998.
8. T. J. R. Hughes. Multiscale phenomena: Green's functions, the Dirichlet-to-Neumann formulation, subgrid scale models, bubbles and the origins of stabilized methods. *Comput. Methods Appl. Mech. Engrg.*, 127(1-4):387–401, 1995.
9. T. J. R. Hughes, G. R. Feijóo, L. Mazzei, and J.-B. Quincy. The variational multiscale method - a paradigm for computational mechanics. *Comput. Methods Appl. Mech. Engrg.*, 166(1-2):3–24, 1998.
10. F. Brezzi, L. P. Franca, T. J. R. Hughes, and A. Russo. $b = \int g$. *Comput. Methods Appl. Mech. Engrg.*, 145(3-4):329–339, 1997.
11. P. E. Barbone and I. Harari. Nearly H^1 -optimal finite element methods. *Comput. Methods Appl. Mech. Engrg.*, 190(43-44):5679–5690, 2001.
12. D. Givoli. Non-local and semi-local optimal weighting functions for symmetric problems involving a small parameter. *Internat. J. Numer. Methods Engrg.*, 26(6):1281–1298, 1988.
13. F. Brezzi and A. Russo. Choosing bubbles for advection-diffusion problems. *Math. Models Methods Appl. Sci.*, 4(4):571–587, 1994.
14. A. Nesliturk and I. Harari. The nearly-optimal Petrov-Galerkin method for convection-diffusion problems. *Comput. Methods Appl. Mech. Engrg.*, 192(22-24):2501–2519, 2003.
15. L. P. Franca, A. L. Madureira, and F. Valentin. Towards multiscale functions: Enriching finite element spaces with local but not bubble-like functions. *Comput. Methods Appl. Mech. Engrg.*, 1940(27-29):3006–3021, 2005.
16. T. Y. Hou and X.-H. Wu. A multiscale finite element method for elliptic problems in composite materials and porous media. *J. Comput. Phys.*, 134(1):169–189, 1997.
17. T. J. R. Hughes and G. Sangalli. Variational multiscale analysis: the fine-scale Green's function, projection, optimization, localization, and stabilized methods. ICES Report 05-46, Institute for Computational Engineering and Sciences, University of Texas at Austin, Austin, Texas, 2005. Submitted to *SIAM J. Numer. Anal.*
18. L. P. Franca, S. L. Frey, and T. J. R. Hughes. Stabilized finite element methods. I. Application to the advective-diffusive model. *Comput. Methods Appl. Mech. Engrg.*, 95(2):253–276, 1992.
19. L. P. Franca and F. Valentin. On an improved unusual stabilized finite element method for the advective-reactive-diffusive equation. *Comput. Methods Appl. Mech. Engrg.*, 189(13-14):1785–1800, 2000.
20. A. A. Oberai and P. M. Pinsky. A residual-based finite element method for the Helmholtz equation. *Internat. J. Numer. Methods Engrg.*, 49(3):399–419, 2000.
21. C. Farhat, I. Harari, and L. P. Franca. The discontinuous enrichment method. *Comput. Methods Appl. Mech. Engrg.*, 190(48):6455–6479, 2001.
22. C. Farhat, I. Harari, and U. Hetmaniuk. The discontinuous enrichment method for multiscale analysis. *Comput. Methods Appl. Mech. Engrg.*, 192(28-30):3195–3209, 2003.
23. V. Gravemeier, W. A. Wall, and E. Ramm. A three-level finite element method for the instationary incompressible Navier-Stokes equations. *Comput. Methods Appl. Mech. Engrg.*, 193(15-16):1323–1366, 2004.
24. A. Deraemaeker, I. Babuška, and P. Bouillard. Dispersion and pollution of the FEM solution for the Helmholtz equation in one, two and three dimensions. *Internat. J. Numer. Methods Engrg.*, 46(4):471–499, 1999.
25. C. Farhat. Private communication. 1996.
26. K. Gosteev. Improved finite element methods for acoustics. Master's thesis, Tel Aviv University, Tel Aviv, Israel, 2005.
27. L. L. Thompson and P. M. Pinsky. A Galerkin least-squares finite element method for the two-dimensional Helmholtz equation. *Internat. J. Numer. Methods Engrg.*, 38(3):371–397, 1995.
28. I. Harari and T. J. R. Hughes. Galerkin/least-squares finite element methods for the reduced wave equation with nonreflecting boundary conditions in unbounded domains. *Comput. Methods Appl. Mech. Engrg.*, 98(3):411–454, 1992.